Mpox virus spreads from cell-to-cell and leads to neuronal injury in human cerebral organoids

Isabel Schultz-Pernice[1,2,3,§], Amal Fahmi[1,2,3,§], Yen-Chi Chiu[4,5], Blandina I. Oliveira Esteves[1,2], Teodora David[1,2], Antoinette Golomingi[1,2], Beatrice Zumkehr[6], Damian Jandrasits[3,7], Roland Züst[7], Selina Steiner[6], Carlos Wotzkow[6], Fabian Blank[6,8], Olivier B. Engler[7], David Baud[4,5], and Marco P. Alves[1,2,9,*]

[1]Institute of Virology and Immunology, Bern, Switzerland

[2]Department of Infectious Diseases and Pathobiology, Vetsuisse Faculty, University of Bern, Bern, Switzerland

[3]Graduate School for Cellular and Biomedical Sciences, University of Bern, Bern, Switzerland

[4]Materno-Fetal and Obstetrics Research Unit, Department "Femme-Mère-Enfant", Lausanne University Hospital, Lausanne, Switzerland

[5]Faculty of Biology and Medicine, University of Lausanne, Lausanne, Switzerland

[6]Department for BioMedical Research, University of Bern, Bern, Switzerland

[7]Spiez Laboratory, Austrasse, 3700 Spiez, Switzerland

[8]Department of Pulmonary Medicine, Inselspital, Bern University Hospital, Bern, Switzerland

[9]Multidisciplinary Center for Infectious Diseases, University of Bern, Bern, Switzerland

[§]These authors contributed equally

*Correspondence: marco.alves@unibe.ch (M.P.A.)

ABSTRACT

In 2022-23 the world experienced the largest recorded mpox virus (MPXV) outbreak outside of endemic regions. Remarkably, cases of neurological manifestations were reported, some of which fatal. MPXV DNA and MPXV-specific IgM antibodies were detected in the cerebrospinal fluid of encephalitis-affected patients, suggesting neuroinvasive potential of MPXV. We explored the susceptibility of neural tissue to MPXV infection using human cerebral organoids (hCOs) exposed to a primary isolate belonging to clade IIb lineage. The virus efficiently replicates in hCOs as indicated by the exponential increase of infectious viral loads and the elevated frequency of MPXV-positive cells over time. Also, electron microscopy imaging revealed the presence of viral particles as well as perinuclear viral factories. We observed susceptibility of several cell lineages to the virus, including neural progenitor cells, neurons, and astrocytes. Furthermore, we detected the presence of viral antigens in neurites and in foci of grouped cells distributed throughout the tissue. In line with this, examining released and cell-associated MPXV titers, we observed significantly more cell-associated infectious virus, suggesting viral spread by cell-to-cell contact. While hCOs displayed no evident outer morphological changes upon infection, we detected the formation of varicosities in neurites, pointing to viral manipulation of axonal transport and neuronal injury. In accordance, the apoptosis marker cleaved caspase-3 was detected within neurite swellings. Our findings identify a mechanism potentially contributing to MPXV-mediated neuropathology that may have therapeutic implications.

Keywords: mpox, monkeypox, orthopoxvirus, zoonosis, neural organoids, cerebral organoids, brain organoids, encephalitis, axonal beading, neuron injury.

INTRODUCTION

The first case of mpox virus (MPXV) infection without traceable contact to African population or fauna was registered in UK in early May 2022[1]. Since then, more than 100 countries reported cases of infection[1], marking the largest recorded MPXV epidemic outside of African countries. First manifestations of MPXV infection observed during the current outbreak include fever, lethargy, myalgia, lymphadenopathy and headache, followed by skin lesion[2-4]. While most clinical cases recorded during the epidemic were observed to be mild[2,4], severe complications may develop. From 1985 to 2021, serious neurological manifestations, including confusion, seizures and encephalitis, have been recorded in around 3% of MPXV infected patients[5], including one fatal case[6]. Since May 2022, encephalitis has been diagnosed in several patients affected by MPXV infection[7-14], including two young, healthy men that died following the complications[7]. Animal studies have suggested neuroinvasive potential of MPXV, detecting viral DNA in the brain of several rodent species[15-18]. This hypothesis is further supported by the detection of MPXV DNA in the cerebrospinal fluid (CSF) of one affected woman during this outbreak[10] as well as the detection of MPXV-specific IgM antibodies in the CSF of a 6-year-old girl in 2003[19].

Despite first reports of deadly encephalitis cases dating back to 1987[6], mechanisms driving acute neurological manifestations during MPXV infections have been poorly investigated in the human host. Possible causes include the previously restricted geographical distribution of the virus, as well as limited availability of material and accurate models to analyze the neuropathology in the human brain. In the past years, advanced three-dimensional (3D) cell culture systems have demonstrated their capability to recapitulate processes shaping human organs in health and disease. Moreover, these *in vitro* systems have provided unprecedented opportunities to study host-pathogen interactions in the human host exploiting a complex system accessible to experimental manipulation. In this study, we evaluated the susceptibility of neural tissue to MPXV infection using human cerebral organoids (hCOs), also known as brain or neural organoids, a sophisticated *in vitro* model closely mimicking human brain.

RESULTS

Neural progenitor cells, astrocytes and neurons are susceptible to mpox virus infection

The generation of hCOs from embryonic stem cells (ESCs) was performed according to established methods (Supplementary Fig. 1a)[20]. To phenotype our cultures, hCO tissue of different developmental stages was sampled over a period of 112 days and processed for immunofluorescence characterization using well-established cell type markers to discriminate between class III β-tubulin (TUJ1) expressing neurons[21-24] and sex-determining region Y-box 2 (SOX2) positive neural progenitor cells (NPCs)[25,26]. During the first days of development, hCOs were observed encompassing high numbers of tightly clustered, small ventricular units, previously described as fluid-filled cavities[20] surrounded by a compact but relatively thin sheath of SOX2-expressing NPCs (Fig 1a, top panels). Isolated TUJ1-positive neurons were occasionally observed scattered around the ventricles. Throughout the first and second month of development, hCOs displayed increasing degrees of complexity, acquiring a typical layered organization[20]. By day 60 of tissue expansion, enlarged ventricles surrounded by several layers of tightly gathered NPCs became evident (Fig. 1a, central panels). Densely packed TUJ1-expressing neurons surrounded the ventricular units, forming a thick meshwork of perikarya and neurites (Fig.1a, central panels). Finally, a nuclei-poor outer layer was observed on the organoid's basal surface (Fig. 1a, central panels). As development progressed further, organoids were observed losing ventricular organization, displaying a scattered population of SOX2-positive cells nested within a neuron-dominated environment (Fig. 1a, bottom panels). Furthermore, astrocytes, characterized by GFAP expression[27] in absence of SOX2 signal, were observed appearing in hCOs by the third month of maturation, in line with previous findings reporting the presence of astrocytes in minor numbers by day 45 of organoid development[28].

Aiming to shed further light on the dynamics of MPXV replication within human neural tissue, we set out to analyze its tropism within our cultures. Four independent batches of hCOs of 70-95 days of age were exposed to a 2022 primary isolate of MPXV belonging to clade IIb lineage. The infected hCOs were processed for immunofluorescence analysis. In line with recent

findings[29], we observed viral antigen localizing to the cytoplasm of SOX2-expressing cells (Fig. 1b, top panels), indicating susceptibility of NPCs to MPXV infection. Likewise, SOX2-negative but GFAP-expressing astrocytes were confirmed to display viral antigen signal within cell somata and extensions (Fig. 1b, central panel). In contrast to previous reports[29], hCO-derived neurons were observed to be susceptible to MPXV infection as well, as viral antigen was identified co-localizing with TUJ1 in both perikarya and neurites (Fig. 1c, bottom panels).

Mpox virus replicates and spreads from cell-to-cell in human cerebral organoids

We next set out to analyze the dynamics of MPXV replication by exposing hCOs to a low multiplicity of infection (MOI) of 0.1 $TCID_{50}$/cell. Images, samples of tissue and supernatant were collected till 10-14 days post-infection (p.i.; Supplementary Fig. 1b). No evident alterations between mock-treated and MPXV-infected cultures were observed in outer morphology at any time point tested. In addition, no significant or pronounced differences emerged through surface area analysis of hCOs, with mock-infected organoids displaying an average surface area over all time points of 13.0 mm^2, with an increase of 5.6 mm^2, compared to MPXV-challenged hCOs, that showed a mean size of 13.4 mm^2 and 4.8 mm^2 growth.

Viral replication and distribution in the tissue over time was investigated through immunofluorescence analysis. Viral particles were highlighted using an antibody targeting the viruses' A27L protein, a conserved and multifunctional viral envelope protein known to mediate viral attachment and fusion to cell surfaces, as well as transport of the related vaccinia virus through microtubule interaction[30-32]. While no viral antigen was visible in mock-treated hCOs, small gatherings of MPXV-positive cells were detected in infected cultures as early as day 2 p.i. (Fig. 2a). Viral antigen signal was subsequently observed steadily increasing over time, reaching a peak at day 10 p.i., at which numerous elliptical and elongated infection foci became evident around the organoid's perimeter (Fig. 2a), alongside streams of infected cells and scattered single cells reaching deep into the hCO core. Between day 10 and day 14 p.i., MPXV signal reached its peak of intensity, as no further increase could be detected (Fig. 2a).

Strikingly, MPXV antigen was observed displaying a clustered distribution with positive cells arranged in delimited foci at the hCO's surface layers (Fig. 2a).

Neural cell susceptibility to MPXV infection was further confirmed via transmission electron microscopy of organoids collected 10 days p.i. Pleomorphic, intracellular mature virions, characterized by a cuboid or ovoid structure with a central biconcave core were clearly visible within cells of the analyzed tissue (Fig. 2b'), and represented the majority of observed viral particles. Intracellular mature virions were visualized both in proximity to viral factories, and approaching the cell's periphery, including regions of cell-to-cell contact. In addition, perinuclear viral factories, containing viral particles at different stages of replication, were observed on multiple occasions (Fig. 2b''). Viral crescent membranes at several stages of maturation were observed, along with immature viral particles, characterized by a smooth membrane encircling material of variable density (Fig. 2b''), previously suggested to indicate different stages of virion organization[33]. Condensed cytoskeletal components were frequently documented in proximity of viral factories (Fig. 2b''). Infected cells were commonly observed in clusters, and displayed features described to appear at advanced stages of viral replication[33], including immature viral particles not only in nuclear proximity but also approaching host cell membrane, sustained nuclear morphology, and cytoskeletal condensations. In addition, we identified cells displaying evident signs of cytopathic effect, with nuclear degeneration and membrane rupture, leading to virus release (Fig. 2c). Extracellular virions without any evident association with cell structures were occasionally observed within hCO tissue. Further stages of viral particle maturation, including intracellular enveloped virions and cell-associated enveloped virions, were not identified.

The vaccinia virus has been described exploiting several mechanisms to spread from cell-to-cell, including the formation of actin tails[34,35] and tunneling nanotubules (TNTs)[36]. Through transmission electron microscopy, we captured viral particles localizing not only to cell somata, but also to tube-like cellular extensions, rich in cytoskeletal components, reminiscent of neurites (Fig. 2d). In line with this observation, detailed immunofluorescence analysis revealed infection not only limited to cell somata, but extending into thin cell filaments, frequently

spanning between two cells within infection foci (Fig. 2e) and disseminated within the organoid's cell meshwork. To elucidate the nature of documented tubular structures, we performed co-localization analysis of viral antigen signal with F-actin and neuronal marker TUJ1, allowing discrimination between TNTs and neurites[37]. Infected filaments of different length staining positive for both F-actin and TUJ1 were detected spanning between cells, confirming MPXV localization within neurites (Supplementary Fig. 2a, yellow arrowheads). In addition, viral antigen accumulation within F-actin positive, but TUJ1 negative cell-connecting filaments, was occasionally observed (Supplementary Fig. 2a, blue arrowheads), suggesting MPXV dissemination into, and possibly through, peripheral cell projections of variable nature. Intrigued by the observed viral distribution within filamentous structures, we set out to investigate the presence of cell-to-cell transmission among hCO cells. To discriminate between released and cell-associated infectious virus, we performed titrations of both supernatant and homogenized hCOs. At all measured time points, cell-associated viral titers were observed to exceed released infectious virus, with differences spanning over several orders of magnitude (Fig. 2f). Significantly higher cell-associated than released viral concentrations were detected across all analyzed batches starting as early as day 2 p.i. and up to day 10 p.i., with most pronounced divergence seen at day 10 p.i. (Fig. 2f). Cell-associated virus consistently contributed to more than 90% of total infectious virus, with percentages fluctuating between 93 and 98% (Fig. 2g).

Mpox virus infection leads to neurite injury in human cerebral organoids

Further analysis of MPXV-infected hCO cultures revealed viral antigen signal accumulating at regular intervals within elliptical swellings along infected filaments (Fig. 3a). Notably, these structures were observed in 100% of independent batches of hCOs processed. Analogous shape modulations, termed neuritic (i.e., axonal or dendritic) beading, have been postulated to indicate degenerative processes and reported to accompany a variety of neuropathologies including Alzheimer's disease, ischemia, and traumatic injuries[38-42]. Beaded filaments were documented spanning for remarkable distances throughout the hCO tissue, both within and

outside of infection foci and swellings were observed to be present in both symmetric, lemon-shaped and clam-shaped, asymmetric morphology, indicative of early and advanced stages of beading[43]. Detailed analysis showed frequent co-localization of viral antigen accumulations with neuronal marker TUJ1, both within swellings and affected filaments, suggesting gathering of viral proteins along dendrites and axons (Fig. 3b). Aiming to confirm the injurious nature of the observed structures, we analyzed the distribution of cleaved caspase-3, a pro-apoptotic protein[44,45], within hCO tissue. In line with previous reports, we observed occasional cleaved caspase-3 accumulation in neuritic varicosities as well as within associated cells (Fig. 3c), supporting apoptotic processes accompanying the beading phenomenon.

DISCUSSION

In this study, we explored the neurobiology of MPXV in the human host using hCOs as an advanced model of the human brain. Our data provides evidence that several neural cell lineages are susceptible to MPXV infection, and the resulting replication leads to virus propagation throughout the cerebral tissue. Moreover, evaluation of infectious virus titers in intra- and extra-cellular compartments indicates a spread of MPXV via cell-to-cell contact in hCOs. The identification of neuronal injury hallmarks and neurodegenerative signs demonstrate the neurovirulence potential of MPXV in humans.

Despite MPXV infection cases being reported since 1970, studies investigating pathomechanisms driving mpox disease are sparse. Moreso, current understanding of processes leading to rare, but often severe complications in mpox affected individuals, shows prominent gaps. We used hCOs of 70 to 95 days of age to model MPXV infection in the human host, as we confirmed that prologued culture allows establishment of relevant cell diversity, encompassing NPCs, neurons and astrocytes, within a highly complex environment. We show that hCOs are highly susceptible to and allow active replication of MPXV, as demonstrated by increasing cell-associated and released infectious virus, transmission electron microscopy, and immunofluorescence. In line with recent reports[46], transmission electron microscopy revealed presence of intracellular viral particles at several documented stages of replication,

including crescent membranes, immature viral particles, intracellular mature viral particles, and extracellular viral particles. These findings show the establishment of MPXV replication machinery in human cerebral tissue is possible and frequently occurs within infected hCO cells. As previously described in Vero cells[33], we observed abundance of intracellular mature virions over all other viral morphotypes, and documented their presence at different subcellular locations, including in close proximity to viral factories, possibly indicating recently formed virions, and adjacent to cell membranes. Furthermore, we confirmed the recurrent presence of bundled cytoskeletal elements, which we frequently observed located in proximity to viral factories. Cytoskeletal rearrangements have been recently reported in MPXV-infected Vero cells[33], and cytoskeleton involvement in processes mediating viral distribution within infected cells has been suggested[32,34,47,48], as well as during cell-to-cell transmission processes, as actin tail formation[34,35,48]. We thus hypothesize that cytoskeletal condensations observed within hCO cells might be involved in MPXV transport within the cell's cytoplasm.

In line with the establishment of a functional viral replication machinery within hCO cells, immunofluorescence analysis showed a steady viral load increase in the course of infection, reaching a peak around day 10 p.i. Viral antigen was initially visualized on the organoid's surface, reaching deep into the tissue at advanced stages of infection. In addition, viral particles were often detected localizing to distinct cell foci or streams, suggesting possible cell-to-cell transmission, a prominent route exploited by orthopoxviruses, as vaccinia virus[34-36]. While no actin tails were visualized by transmission electron microscopy, intracellular mature viral particles were observed within neurite sections in the processed tissue. In addition, immunofluorescence analysis showed viral antigen localizing not only to cell somata, but also to filaments of variable length, connecting distinct cells and dispersed within the organoid tissue. Characterization of the strands showed that both TUJ1 positive neurites and F-actin positive, but TUJ1 negative TNTs are found harboring viral particles within hCOs, suggesting cell-to-cell transmission might occur through different routes in human neural tissue. Comparison of cell-associated and released infectious virus further strengthened this assumption. Indeed, intracellular viral loads were found to significantly exceed the amount of

220 released virus till day 10 p.i., with cell-associated viral particles steadily representing over 90%
221 of total infectious virus present in tissue and culture supernatant. Together, our findings
222 suggest that, as previously documented for the closely related vaccinia virus, MPXV
223 preferentially spreads directly from cell-to-cell and can exploit different mechanisms to spread
224 within human neural tissue. Furthermore, while our observations confirm the possible
225 transmission of MPXV through TNTs, as earlier documented for vaccinia virus[36], we
226 predominantly detected localization of viral antigen within TUJ1 positive neurites. This
227 observation suggests a previously undocumented mode of viral transmission for MPXV in the
228 human brain, in which viral particles can be transported from one cell to another through axons
229 and dendrites. Documented cytoskeletal alterations in proximity to viral factories could hint at
230 the mechanism of transportation of the virus, which could exploit the cell's fast axonal transport
231 machinery to move through the cytosol and reach distant locations, a mechanism observed to
232 be exploited by viruses of several families, most prominently *Herpesviridae*, *Flaviviridae*,
233 *Rhabdoviridae* and *Picornaviridae*[49], allowing viral dissemination while evading the host's
234 immune system.
235 In addition, our findings suggest possible injurious consequences of viral spread within cell
236 extensions. Viral antigen-containing filaments were often observed showing a series of
237 sequential swellings, termed neuritic beads. Analogous varicosities have been documented to
238 accompany diverse pathological states, including neurodegenerative disorders such as
239 Alzheimer's disease[38,39], ischemia[40] , traumatic injuries[41,42] and neurotropic virus infections[50-
240 [52]. Beads are thought to originate from changes in membrane tension, and organelles,
241 cytoskeletal components as well as pathology-associated proteins have been observed to
242 sporadically pause or accumulate within them[43,53]. In line with these observations, we
243 confirmed occasional accumulation of cleaved caspase-3 within the somata and axonal
244 swellings of infected cells. Furthermore, varicosities have been observed to appear on axons
245 of trigeminal neurons upon pseudorabies virus cell attachment[54]. These swellings have been
246 suggested to represent sites of virus egress[54], promoting cell-to-cell spread[55], and could
247 possibly be accompanied by a deleterious interference with regular axonal functions[56]. It

seems reasonable to hypothesize that MPXV hijacks the cell's transport machinery, causing cytoskeletal rearrangement, and exploits it to move through axons, leading to the generation of neuritic beads that might represent sites of viral egress, finally causing neuronal injury by hampering cell functions. Our findings furthermore indicate that cell death, and more precisely apoptosis of infected neurons, can be triggered merely by viral presence in the absence of immune cells. Future studies, focusing on elucidating the transport and egress dynamics of MPXV within axons as well as the timing and process of bead formation, possibly through high-resolution live-cell imaging of fluorescently tagged virions, will be required to fully comprehend the underlying mechanisms and consequences of our findings.

Recently, Chailangkarn and colleagues, found induced pluripotent stem cell-derived neural progenitor cells and astrocytes to be susceptible to MPXV infection in a two-dimensional culture environment. This was demonstrated by changes in cell morphology and viability, as well as increased viral loads detected in supernatant by qPCR over time[29]. In contrast, 14 and 45-day old neurons did not show productive MPXV infection[27]. In an unrefereed preprint, human pluripotent stem cell-derived cortical neurons were however shown to be permissive to MPXV infection by Bauer and colleagues, even if at a lower degree compared to astrocytes and microglia[57]. In line with both reports, we confirmed susceptibility of both NPCs and astrocytes to MPXV infection and found TUJ1-expressing neurons to be permissive to MPXV infection as well. We propose that the prevalence of cell-associated neuronal spread of MPXV through axonal transport provides a rationale for the previously reported low or undetected viral replication within human neurons, suggested to resist viral infection to a certain degree, based on the lack of strong increased detectable virus in culture supernatant. Further investigation of the exact mechanisms driving the observed phenomenon could prove of utmost importance in the development and identification of novel treatment options for patients affected by MPXV encephalitis.

Taken together, we show that human neural tissue, modelled in a complex 3D environment, is highly susceptible to infection with a contemporary clade IIb lineage MPXV isolate. We show that viral replication factories are successfully established, resulting in a productive replication

of MPXV within organoid cells. Furthermore, we find that viral antigen localizes not only to cell somata, but also to filaments of variable nature. We propose that MPXV preferentially spreads from cell-to-cell, exploiting not only previously described mechanisms, but also through axonal transport. Our hypothesis is further corroborated by the observation of serial swellings along filaments, previously documented to represent sites of virus egress and cell-to-cell transmission, as well as a sign of neuronal injury. Our findings identify a mechanism of MPXV spread in the human cerebral tissue and constitute the basis for further exploration of the neurobiology of orthopoxviruses.

MATERIAL AND METHODS

Ethics statement

In accordance with Articles 13 and 14 of the Federal Act on Research on Embryonic Stem Cells, and Article 20 of the Ordinance on Research on Embryonic Stem Cells, the work with human H1 ESC line was approved by the Cantonal Ethics Committee of Bern, Switzerland under the authorization number R-FP-S-2-0023-0000.

Maintenance of human embryonic stem cells

The human H1 ESC line (WiCell) was cultured in feeder-free conditions and used to generate hCOs employed in this study. ESCs were seeded onto untreated culture flasks (Sigma-Aldrich) coated with Vitronectin XF (Stem Cell Technologies) and maintained in mTeSR Plus medium (Stem Cell Technologies). Cells were maintained according to the manufacturer's recommendations. Cells were passaged every 6-7 days applying 0.5 mM EDTA (Thermofisher) in sterile Dulbecco's Phosphate Buffered Saline (DPBS, Gibco) for 4 minutes at 37°C, 5% CO_2, followed by mechanical dissociation to obtain aggregates encompassing approximately 5-8 cells. Regions with differentiated cells were scratched prior to cell detachment. Cells were regularly checked and found negative for mycoplasma contamination.

Generation of human cerebral organoids

hCOs were generated using an adapted version of the previously published protocol by Lancaster and colleagues[58]. Briefly, on day 0, ESCs were detached applying Accutase (Sigma-Aldrich) for 4 minutes at 37 °C, 5% CO_2. Cells were dissociated by repeated pipetting till a single-cell suspension was obtained. Cells were counted, centrifuged at 200 g for 5 minutes at room temperature, and resuspended in the required volume of Formation Medium prepared using the STEMdiff Cerebral Organoid Kit (Stem Cell Technologies) supplemented with 50 µM Rho-associated protein kinase (ROCK) inhibitor Y-27632 (Stem Cell Technologies). The cell suspension was distributed into ultra-low attachment 96-well plates (Corning), each well containing 9'000 to 10'000 cells suspended in 100 uL of Formation Medium. The cultures were left undisturbed for at least 24 hours. On day 2 and 4, 100 µL/well of Formation Medium without ROCK inhibitor were added. On day 5, the formation of embryoid bodies (EBs) was confirmed and EBs were transferred with wide-bore 200 uL tips to ultra-low attachment 24-well plates (Corning), previously filled with 500 µL/well of Induction Medium, prepared using the STEMdiff Cerebral Organoid Kit. On day 7, EBs were embedded into 30 µL droplets of Matrigel (Corning) each and transferred into ultra-low attachment 6-well plates (Corning) containing 3 mL of home-made Expansion Medium consisting of a 1:1 mixture of DMEM/F-12 (Gibco) and Neurobasal Medium (Gibco) supplemented with 1:200 N2 (Gibco), 1:100 B27 minus vitamin A (Gibco), 2.5 µg/mL insulin (Sigma-Aldrich), 1:100 GlutaMAX (Gibco), 1:200 MEM-NEAA (Seraglob), 3.5 µL/L 2-mercaptoethanol (Sigma-Aldrich), and 1:100 Penicillin-Streptomycin (Sigma-Aldrich, Gibco). On day 10, Expansion Medium was gently removed and replaced with 3.5 mL homemade differentiation medium consisting of a 1:1 mixture of DMEM/F-12 and Neurobasal medium supplemented with 1:200 N2, 1:100 B27, 2.5 µg/mL insulin, 1:100 GlutaMAX, 1:200 MEM-NEAA, 3.5 uL/L 2-mercaptoethanol, 1:100 Penicillin-Streptomycin, and 0.5 ug/mL Amphotericin B (Gibco). From day 10 on, hCOs were cultured on an orbital shaker at 65 rpm, in a 37 °C, 5% CO_2 incubator. Medium was changed every 2 to 3 days. hCOs between 70-95 days old that passed the quality control criteria[58] were used for the experiments. Criteria included hESC stemness of at least 80% of double positive cells for both stemness markers SSEA-1 (Stem Cell Technologies) and TRA-1-60 (Stem Cell Technologies), which

was measured at day 0 by flow cytometry (FCM) assay. FCM acquisitions were performed on a FACS Canto II (BD Bioscience) using the DIVA software and further analyzed with FlowJo (TreeStar). Further quality control criteria included typical sizes corresponding to each developing stage, brightening of outer layer at the EBs stage before embedding, and formation of neural tube-like structures in Matrigel. All used media were warmed to room temperature (20-25°C) before usage.

Mpox virus propagation

A primary isolate of MPXV belonging to clade IIb lineage isolated in 2022 was used for this study (kindly provided by Prof. Dr. Isabela Eckerle, Geneva Center for Emerging Viral Diseases and Division of Infectious Diseases, University Hospital of Geneva). The MPXV isolate was passaged three times on Vero E6 cells to produce virus stocks. Briefly, 24 hours prior to infection, Vero E6 cells were seeded in 75 cm^2 tissue culture flasks (TPP), at a density of $8x10^6$ cells per flask, and cultured at 37°C, 5% CO_2 in DMEM supplemented with GlutaMAX (Gibco), 10% fetal bovine serum (FBS, Gibco), 1 mM Sodium Pyruvate (Gibco) and 10 mM HEPES (Gibco). On the day of infection, the culture medium was replaced with 5 mL of DMEM supplemented with GlutaMAX and 2% FBS, and the required amount of virus stock was added. Cells were placed on an orbital shaker moving at 60 rpm for 1 hour at 37°C, 5% CO_2. Following incubation, 15 mL DMEM supplemented with GlutaMAX and 2% fetal bovine serum were added. Cells were incubated at 37°C, 5% CO_2 and inspected daily for signs of cytopathic effect (CPE). At day 3 p.i. (i.e., when a CPE of around 80% of cells was observed) flasks were frozen at -70°C, to release cell-associated viral particles. Viral suspensions were subsequently thawed, collected in 50 mL conical tubes, and centrifuged at 1000 g for 10 minutes at 4°C to remove cell debris. Supernatants were aliquoted and stored at -70°C till further use. Mock control stocks were generated in parallel, following the same procedures, with omission of virus inoculum. All procedures involving MPXV handling were carried out in biosafety level 3 (BSL3) conditions at the Institute of Virology and Immunology (University of Bern, Switzerland) by trained personnel provided with appropriate personal protective equipment.

360

361 **Mpox virus titration**

362 Viral stocks, organoid supernatants and homogenized organoids were titrated on Vero E6 cells
363 in a 96-well plate format. 24 hours prior to titration, the required number of 96 well plates (TPP)
364 were seeded with a suspension of Vero E6 cells at a density of $2x10^4$ cells per well. Serial
365 dilutions were performed in DMEM supplemented with GlutaMAX, 10% FBS,1 mM Sodium
366 Pyruvate, 10 mM HEPES (Gibco), and 1% Penicillin-Streptomycin, starting at a dilution of 1:10.
367 Cell supernatant was aspirated, and the dilutions transferred on the previously seeded cells.
368 Cells were incubated for 72 hours at 37°C, 5% CO_2. For readout, the inoculum was aspirated,
369 cells washed once with 200 µL PBS (Sigma-Aldrich), fixed for 15 minutes by immersion in 4%
370 paraformaldehyde (PFA, Sigma-Aldrich), and subsequently stained for 10 minutes with crystal
371 violet. Plates were washed with tap water and left to dry prior to readout. Viral titers were
372 calculated as $TCID_{50}$ per mL using the Reed and Muench method. For titration of released viral
373 loads, culture supernatant was collected at selected time points and stored at -70°C until
374 further analysis. Analogously, for quantification of cell-associated infectious virus, one
375 organoid per time
376 point was randomly sampled, washed with sterile DPBS and transferred into a 1.5 mL screw
377 cap tube containing 1 mL of sterile DPBS. The sample was frozen at -70°C. For analysis, the
378 thawed hCO was dissociated thoroughly by pipetting up and down, until no cell clumps were
379 visible any longer. The sample was centrifuged at 450 g for 5 minutes at 4°C and the
380 supernatant used for titration. For normalization, obtained released viral titers were multiplied
381 by the volume of medium per well and divided by the number of hCOs per well, to obtain
382 released infectious virus per hCO. Analogously, cell-associated viral titers were multiplied by
383 the total sample volume and divided by the number of organoids per sample, to obtain cell-
384 associated infectious virus per hCO.

385

386 **Human cerebral organoids infection**

hCOs were infected at 70 to 95 days of age in a 6-well plate format with an MOI of 0.1 $TCID_{50}$/cell. Briefly, virus suspension was prepared by adding the required amount of virus stock to organoid Maturation Medium (see "Generation of human cerebral organoids") in a 50 mL conical tube to obtain a homogeneous suspension of 3 mL per well. Mock treatment was prepared analogously. Organoid culture medium was removed from all wells and replaced with the inoculum. hCOs were incubated for 2 hours at 37°C, 5% CO_2, constantly shaking at 65 rpm. hCOs were subsequently washed three times with 3 mL of sterile DPBS. 4 mL of fresh organoid Maturation Medium were added to each well, and hCOs were placed back in the incubator at 37°C, 5% CO_2, shaking at 65 rpm. Supernatant samples were taken 2 hours post washing to confirm baseline infectious viral loads. Further tissue and culture supernatant samples were collected at selected time points and stored at -70°C until further analysis. All media and reagents were allowed to reach room temperature prior to application of hCOs.

Human cerebral organoids cryopreservation and immunofluorescence

hCOs were processed using an adapted version of the protocol "Cryogenic Tissue Processing and Section Immunofluorescence of Cerebral Organoids" provided by STEMCELL Technologies. For immunofluorescence, hCOs were washed twice with PBS and fixed in 4% PFA. Next, hCOs were washed three times with PBS. For cryogenic preservation, hCOs were subsequently incubated at 4°C in a 30% sucrose (Sigma-Aldrich) in PBS solution until organoids were observed to sink to the bottom of the tube. Equilibrated hCOs were embedded and incubated in a 7.5% gelatin, 10% sucrose in PBS solution for 1 hour at 37°C, to avoid polymerization. In the meantime, a mixture of dry ice and 100% ethanol was prepared. hCOs and gelatin were subsequently transferred to a Crymold (Biosystems Switzerland AG) and, after initial polymerization at room temperature, carefully placed on the surface of the (no longer boiling) mixture of dry ice and ethanol. Once completely frozen, embedded hCOs were transferred to -80°C for long term storage. For immunofluorescence, cryopreserved hCOs were processed into 18 µm thin slices using a Leica CM1950 cryostat and placed on SuperFrost Plus Adhesion slides (Epredia). Slides were stored at -20°C till staining. For

staining, sections were allowed to reach room temperature prior to processing. To dissolve gelatin, slides were subsequently incubated for 10 minutes in a 37°C pre-warmed mixture of 0.1% Tween-20 (Sigma-Aldrich) in PBS. hCO sections were encircled using a ReadyProbes Hyrophobic Barrier Pap Pen (Thermo Fisher Scientific) and blocked with a 5% donkey serum (Abcam) in 0.1% Tween-20 in PBS solution for 1 hour at room temperature. Primary antibodies were resuspended in 0.1% Tween-20 in PBS supplemented with 5% BSA at the following dilutions: TUJ1 (BioLegend, 801202, 1:400), SOX2 (Invitrogen, 14-9811-82, 1:200), GFAP (Invitrogen, PA1-10004, 1:200), vaccina virus i.e. MPXV A27L protein (OriGene Technologies, Inc BP1076, 1:1000), cleaved caspase-3 (arigo Biolaboratories Crop., ARG66888, 1:200). Blocking buffer was removed, 100 uL of primary antibody solution were added to each section and slides were allowed to incubate at 4°C overnight. On the following day, primary antibody solution was removed by gently tapping slides on paper towels and sections were washed three times for 5 minutes by immersion in 0.1% Tween-20 in PBS. Secondary antibodies were resuspended in 0.1% Tween-20 in PBS at the following dilutions: anti-mouse AF488 (Invitrogen, A21131, 1:200), anti-mouse AF647 (Invitrogen, A2124, 1:200), anti-rat AF647 (Invitrogen, A21247, 1:500), anti-chicken AF546 (Invitrogen, A11040, 1:200), anti-rabbit AF488 (Jackson ImmunoResearch Europe Ltd., 711-545-152, 1:200), anti-rabbit AF546 (Invitrogen, A11035, 1:200), anti-rabbit AF647 (Invitrogen, A21245, 1:200). For nuclear and F-actin staining, DAPI (Sigma-Aldrich) and Rhodamine Phalloidin (Invitrogen, R415, 1:200) were added to the mixture. Sections were incubated with secondary antibodies for 2 hours at room temperature. Slides were subsequently washed three more times for 5 minutes by immersion in 0.1% Tween-20 in PBS and mounted in EMS Shield Mount with DABCO (Electron Microscopy Sciences). Imaging was performed using a Carl Zeiss LSM710 confocal microscope at the microscopy imaging center (MIC) of the University of Bern, Switzerland. Images were analyzed using ImageJ.

Transmission electron microscopy

For transmission electron microscopy, hCOs were fixed using a 2.5% glutaraldehyde and 2% PFA solution in organoid Maturation Medium for a duration of 1 day at 4°C. Subsequently, the fixation solution was replaced with 4% PFA, and samples stored at 4°C until further processing. hCOs were cut into 1 mm3 cubes and immerged in a 1% osmium tetroxide (Electron Microscopy Sciences) solution in ddH_2O for 1 hour at room temperature. After washing three times with ddH_2O, samples were progressively dehydrated in a graded ethanol series, starting from 50% and progressing to 70%, 80%, 90%, and finally 100% ethanol. The samples were then embedded in epoxy resin (EM0300, Sigma-Aldrich) and left to polymerize for 8 hours at 70℃. Ultrathin sections of resin-embedded tissue were prepared using a Leica EM UC7 ultramicrotome. Sections of 70 nm were collected on EM grids (G100H-Cu, Electron Microscopy Sciences) and processed using a 2% uranyl acetate and 0.5% lead citrate solution for contrast enhancement. The obtained sections were imaged using a CM-100 transmission electron microscope (Philips) at 80 kV. Images were analyzed using ImageJ.

Statistical analysis

GraphPad Prism 9 software was used for statistical analysis and graph generation. Non-parametrical Mann-Whitney U test was used to assess significance of detected values. $p<0.05$ was considered statistically significant.

ACKNOWLEDGEMENTS

We would like to extend our gratitude to the Geneva Center for Emerging Viral Diseases, the Division of Infectious Diseases and Prof. Dr. Isabela Eckerle for providing the clade IIb MPXV isolate used in this study. This work was supported by a grant from the Multidisciplinary Center for Infectious Diseases of the University of Bern (to M.P.A.) and by intramural funding of the Institute of Virology and Immunology.

DECLARATION OF INTEREST

The authors declare no competing interests.

DATA AVAILABILITY STATEMENT

The data generated and analyzed during the current study are available from the corresponding author on reasonable request.

AUTHOR CONTRIBUTIONS

I.S.P., A.F., D.B., and M.P.A. conceptualized and designed the project. I.S.P., A.F., Y.C.C., B.O.I.E., T.D., and B.Z. conducted the investigations. I.S.P., A.F., Y.C.C., B.O.I.E., T.D., B.Z., A.G., S.S., C.W., R.Z. D.J., F.B., and O.B.E. developed the methodology and provided reagents. M.P.A., I.S.P., A.F., Y.C.C., B.O.I.E., and T.D. curated and analyzed the data. I.S.P., A.F., and M.P.A. wrote the original manuscript. All authors reviewed, edited, and approved the manuscript.

REFERENCES

1. Organization, W.H. 2022 Mpox (Monkeypox) Outbreak: Global Trends. (2022).
2. Thornhill, J.P., *et al.* Monkeypox Virus Infection in Humans across 16 Countries - April-June 2022. *The New England Journal of Medicine* **387**, 679-691 (2022).
3. Perez Duque, M., *et al.* Ongoing monkeypox virus outbreak, Portugal, 29 April to 23 May 2022. *Eurosurveillance* **27**(2022).
4. Girometti, N., *et al.* Demographic and clinical characteristics of confirmed human monkeypox virus cases in individuals attending a sexual health centre in London, UK: an observational analysis. *The Lancet Infectious Diseases* **22**, 1321-1328 (2022).
5. Badenoch, J.B., *et al.* Neurological and psychiatric presentations associated with human monkeypox virus infection: A systematic review and meta-analysis. *EClinicalMedicine* **52**, 101644 (2022).
6. Jezek, Z., Szczeniowski, M. & Paluku, K.M. Human Monkeypox: Clinical Features of 282 Patients. *The Journal of Infectious Diseases* **156**, 2 (1987).
7. Kozlov, M. How deadly is monkeypox? What scientists know. *Nature* **609**, 663 (2022).
8. Pastula, D.M., *et al.* Two Cases of Monkeypox-Associated Encephalomyelitis - Colorado and the District of Columbia, July-August 2022. *Morbidity and Mortality Weekly Report* **71**, 1212 - 1215 (2022).

9. Viguier, C., *et al.* A severe monkeypox infection in a patient with an advanced HIV infection treated with tecovirimat: clinical and virological outcome. *International Journal of Infectious Diseases* **125**, 135-137 (2022).

10. Cole, J., *et al.* Monkeypox encephalitis with transverse myelitis in a female patient. *Lancet Infect Dis* (2022).

11. Rodriguez, A., Rodriguez, L.C. & Bastidas, N. Acute disseminated encephalomyelitis in a patient with monkeypox: a case report and radiological findings. *Emerging Radiology* (2022).

12. Marin-Medina, D.S., *et al.* Encephalomyelitis in a patient with monkeypox: an unusual complication. *Journal of Neurovirology* **29**, 237-240 (2023).

13. Sharma, R., Nguyen-Luu, T., Dhaubhadel, P., Sharma, A. & Naik, R. A Rare Co-occurrence of Monkeypox Encephalitis and Neurosyphilis. *Cureus* **15**, e35945 (2023).

14. Yadav, P.D., *et al.* An imported case of fatal encephalitis associated with mpox virus infection, India, July 2022. *Journal of Medical Virology* **95**, e28755 (2023).

15. Huston, C.L., *et al.* Monkeypox zoonotic associations: insights from laboratory evaluation of animals associated with the multi-state us outbreak. *The American Journal of Tropical Medicine and Hygiene* **76**(2007).

16. Kulesh, D.A., *et al.* Monkeypox virus detection in rodents using real-time 3'-minor groove binder TaqMan assays on the Roche LightCycler. *Laboratory Investigation* **84**, 1200-1208 (2004).

17. Falendysz, E.A., *et al.* Evaluation of monkeypox virus infection of black-tailed prairie dogs (Cynomys ludovicianus) using in vivo bioluminescent imaging. *Journal of Wildlife Diseases* **50**, 524-536 (2014).

18. Hutson, C.L., *et al.* Monkeypox disease transmission in an experimental setting: prairie dog animal model. *PLoS One* **6**, e28295 (2011).

19. Sejvar, J.J., *et al.* Human Monkeypox Infection: A Family Cluster in the Midwestern United States. *The Journal of Infectious Diseases* **190**, 1833-1840 (2004).

20. Lancaster, M.A., *et al.* Cerebral organoids model human brain development and microcephaly. *Nature* **501**, 373-379 (2013).

21. Sullivan, K.F. & Cleveland, D.W. Identification of conserved isotype-defining variable region sequences for four vertebrate beta tubulin polypeptide classes. *The Proceedings of the National Academy of Sciences* **83**, 4327-4331 (1986).

22. Sullivan, K.F. Structure and Utilization of Tubulin Isotypes. *Annual review of cell biology* **4**, 687-716 (1988).

23. Burgoyne, R.D., Cambray-Deakin, M.A., Lewis, S.A., Sarkar, S. & Cowan, N.J. Differential distribution of beta-tubulin isotypes in cerebellum. *The EMBO Journal* **7**, 2311-2319 (1988).

24. Lee, M.K., Tuttle, J.B., Rebhun, L.I., Cleveland, D.W. & Frankfurter, A. The Expression and Posttranslational Modification of a Neuron-Specific beta-Tubulin Isotype During Chick Embryogenesis. *Cell Motility and the Cytoskeleton* **17**, 118-132 (1990).

25. Zappone, M.V., *et al.* Sox2 regulatory sequences direct expression of a β-geo transgene to telencephalic neural stem cells and precursors of the mouse embryo, revealing regionalization of gene expression in CNS stem cells. *Development* **127**, 2367-2382 (2000).

26. Graham, V., Khudyakov, J., Ellis, P. & Pevny, L. SOX2 functions to maintain neural progenitor identity. *Neuron* **39**, 749-765 (2003).

27. Eng, L.F., Vanderhaeghen, J.J., Bignami, B. & Gerstl, B. An acidic protein isolated from fibrous astrocytes. *Brain Research* **28**(1971).

28. Nascimento, J.M., *et al.* Human Cerebral Organoids and Fetal Brain Tissue Share Proteomic Similarities. *Frontiers in Cell and Developmental Biology* **7**, 303 (2019).

29. Chailangkarn, T., *et al.* Monkeypox virus productively infects human induced pluripotent stem cell-derived astrocytes and neural progenitor cells. *Journal of Infection* **85**, 702-769 (2022).

30. Doms, R.W., Blumenthal, R. & Moss, B. Fusion of Intra- and Extracellular Forms of Vaccinia Virus with the Cell Membrane. *Journal of Virology* **64**, 4884-4892 (1990).

31. Chung, C.-S., Hsiao, Y.-C., Chang, U.-S. & Chang, W. A27L Protein Mediates Vaccinia Virus Interaction with Cell Surface Heparan Sulfate. *Journal of Virology* **72**, 1577–1585 (1998).

32. Sanderson, C.M., Hollinshead, M. & Smith, G.L. The vaccinia virus A27L protein is needed for the microtubuledependent transport of intracellular mature virus particles. *Journal of General Virology* **81**, 47-58 (2000).

33. Witt, A.S.A., *et al.* Ultrastructural analysis of monkeypox virus replication in Vero cells. *Journal of Medical Virology* **95**, e28536 (2023).

34. Stokes, G.V. High-Voltage Electron Microscope Study of the Release of Vaccinia Virus from Whole Cells. *Journal of Virology* **18**(1976).

35. Cudmore, S., Cossartt, P., Griffiths, G. & Way, M. Actin-based motility of vaccinia virus. *Nature* **378**, 636–638 (1995).

36. Xiao, M., Xu, N., Wang, C., Pang, D.W. & Zhang, Z.L. Dynamic monitoring of membrane nanotubes formation induced by vaccinia virus on a high throughput microfluidic chip. *Scientific Reports* **7**, 44835 (2017).

37. Valappil, D.K., Raghavan, A. & Nath, S. Detection and Quantification of Tunneling Nanotubes Using 3D Volume View Images. *Journal of Visualized Experiments* (2022).

38. Ohgami, T., Kitamoto, T. & Tateishi, J. Alzheimer's amyloid precursor protein accumulates within axonal swellings in human brain lesions. *Neuroscience Letters* **136**, 75-78 (1992).

39. Wirths, O., Weis, J., Szczygielski, J., Multhaup, G. & Bayer, T.A. Axonopathy in an APP/PS1 transgenic mouse model of Alzheimer's disease. *Acta Neuropathologica* **111**, 312-319 (2006).

40. Hori, N. & Carpenter, D.O. Functional and Morphological Changes Induced by Transient in Vivo Ischemia. *Experimental Neurology* **129**, 279-289 (1994).

41. Pavlidis, M., Stupp, T., Naskar, R., Cengiz, C. & Thanos, S. Retinal Ganglion Cells Resistant to Advanced Glaucoma: A Postmortem Study of Human Retinas with the Carbocyanine Dye DiI. *Investigative Ophthalmology & Visual Science* **44**, 5196-5205 (2003).

42. Li, Y.*, et al.* A Precise, Controllable in vitro Model for Diffuse Axonal Injury Through Uniaxial Stretch Injury. *Frontiers in Neuroscience* **13**, 1063 (2019).

43. Datar, A.*, et al.* The Roles of Microtubules and Membrane Tension in Axonal Beading, Retraction, and Atrophy. *Biophysical Journal* **117**, 880-891 (2019).

44. Fernandes-Alnemri, T., Litwack, G. & Alnemri, E.S. CPP32, a novel human apoptotic protein with homology to Caenorhabditis elegans cell death protein Ced-3 and mammalian interleukin-1 beta-converting enzyme. *Journal of Biological Chemistry* **269**, 30761-30764 (1994).

45. Waterhouse, N.*, et al.* Heteronuclear ribonucleoproteins C1 and C2, components of the spliceosome, are specific targets of interleukin 1beta-converting enzyme-like proteases in apoptosis. *J Biol Chem* **271**, 29335-29341 (1996).

46. Ormel, P.R.*, et al.* Microglia innately develop within cerebral organoids. *Nature Communications* **9**, 4167 (2018).

47. Hiller, G., Weber, K., Schneider, L., Parajsz, C. & Jungwirth, C. Interaction of assembled progeny pox viruses with the cellular cytoskeleton. *Virology* **98**, 142-153 (1979).

48. Hollinshead, M.*, et al.* Vaccinia virus utilizes microtubules for movement to the cell surface. *Journal of Cell Biology* **154**, 389-402 (2001).

49. Taylor, M.P. & Enquist, L.W. Axonal spread of neuroinvasive viral infections. *Trends in Microbiology* **23**, 283-288 (2015).

50. Jacomy, H., Fragoso, G., Almazan, G., Mushynski, W.E. & Talbot, P.J. Human coronavirus OC43 infection induces chronic encephalitis leading to disabilities in BALB/C mice. *Virology* **349**, 335-346 (2006).

51. Hirano, M.*, et al.* Tick-borne flaviviruses alter membrane structure and replicate in dendrites of primary mouse neuronal cultures. *Journal of General Virology* **95**, 849-861 (2014).

52. Jackson, A.C. Diabolical effects of rabies encephalitis. *Journal of Neurovirology* **22**, 8-13 (2016).

53. Yong, Y., Hunter-Chang, S., Stepanova, E. & Deppmann, C. Axonal spheroids in neurodegeneration. *Molecular and Cellular Neuroscience* **117**, 103679 (2021).

54. De Regge, N.*, et al.* Alpha-herpesvirus glycoprotein D interaction with sensory neurons triggers formation of varicosities that serve as virus exit sites. *The Journal of Cell Biology* **174**, 267-275 (2006).

55. Tomishima, M.J. & Enquist, L.W. In vivo egress of an alphaherpesvirus from axons. *Journal of Virology* **76**, 8310-8317 (2002).

56. Hatch Berth, S., Leopold, P.L. & Morfini, G. Virus-induced neuronal dysfunction and degeneration. *Frontiers in Bioscience-Landmark* **14**(2009).

622 57. Bauer, L., *et al.* Dissecting the neurotropism and neurovirulence of MPXV using human
623 stem cell-based models. *bioRxiv* (2023).

624 58. Lancaster, M.A. & Knoblich, J.A. Generation of cerebral organoids from human
625 pluripotent stem cells. *Nat Protoc* **9**, 2329-2340 (2014).
626

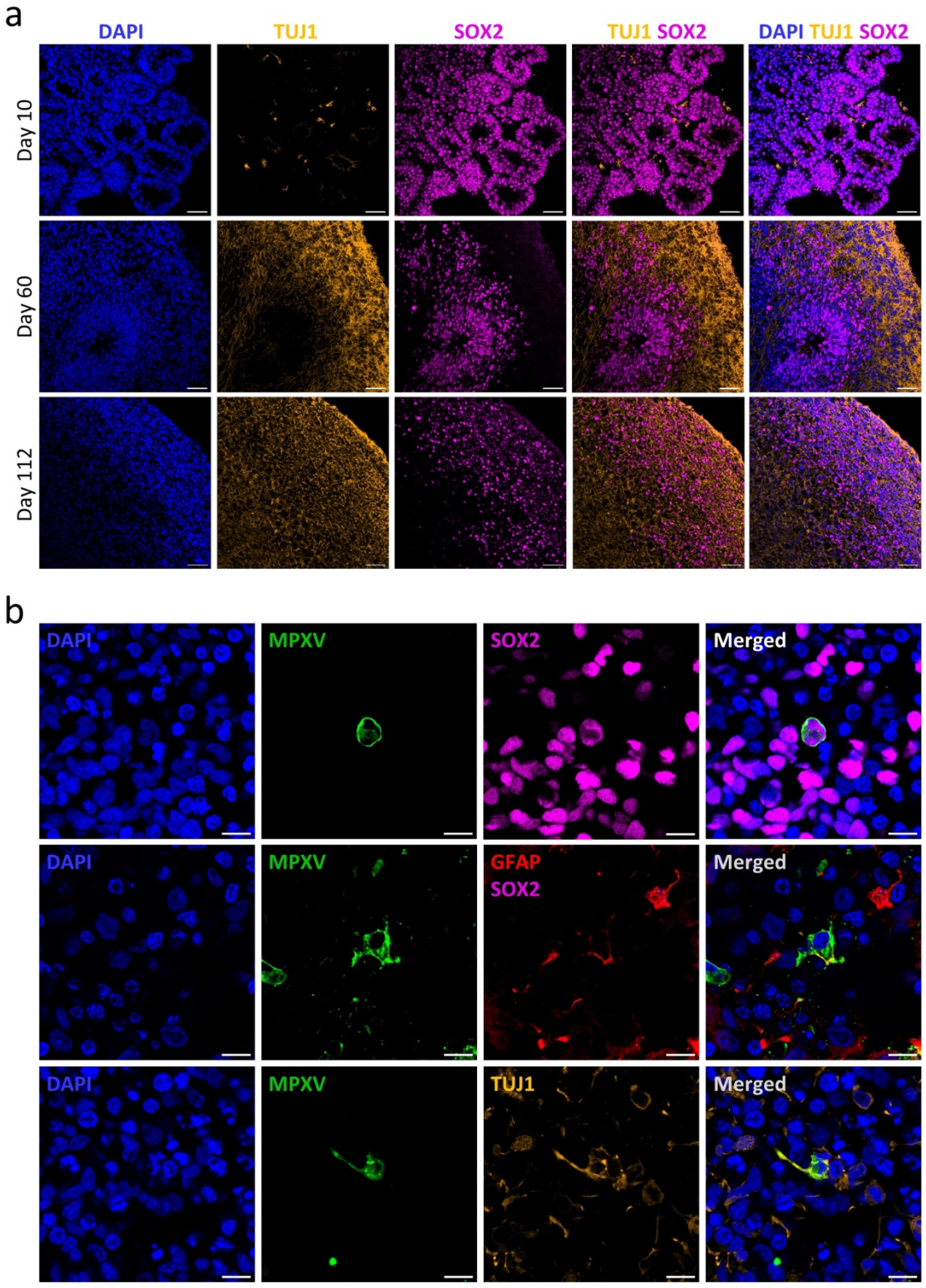

Figure 1: MPXV has a broad cellular tropism in hCOs. (a) Representative micrographs showing the cell diversity and morphology of ESC-derived hCOs at selected developmental time points (10, 60, and 112 days). Selected markers of neural progenitors (SOX2, pink) and neurons (TUJ1, yellow) are presented. DAPI, blue. Scale bar, 50 µm. (b) Representative micrographs illustrating the target cells of MPXV in 70-95 days old hCOs 10 days p.i. with a

633 clade IIb lineage isolate at a MOI of 0.1 $TCID_{50}$/cell. MPXV, green; SOX2, pink; GFAP, red;

634 DAPI, blue. Scale bar, 10 μm.

635

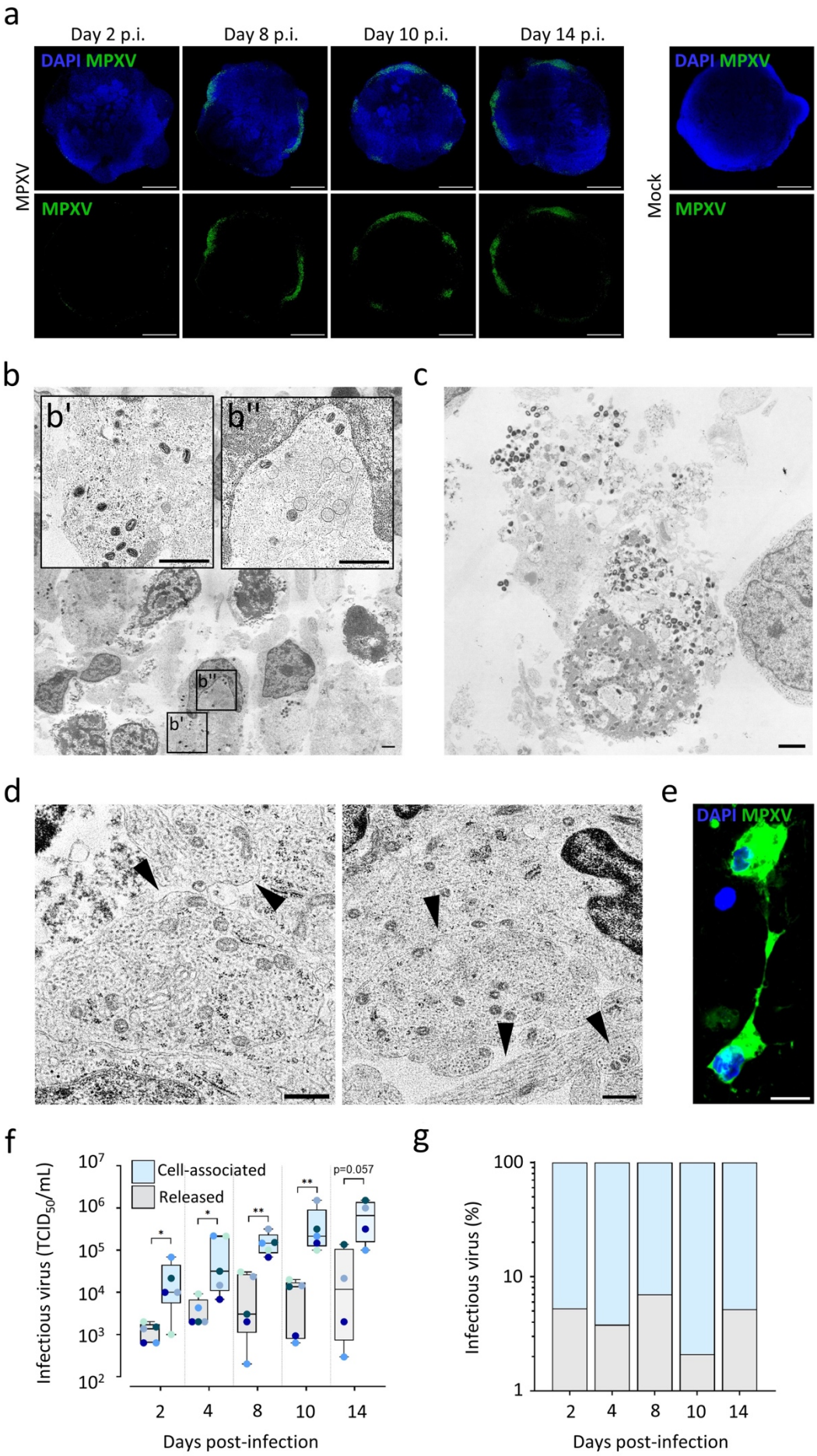

636

637 **Figure 2: Productive MPXV infection and cell-to-cell transmission in hCOs.** (a)
638 Representative micrographs of 70-95 days old hCOs infected with a clade IIb lineage MPXV
639 isolate at a rate of 0.1 $TCID_{50}$/cell. Infection was followed by immunofluorescence from 2 to 14
640 days p.i. by whole-organoid imaging. MPXV, green; DAPI, blue. Scale bar, 1000 µm. (b-d)
641 Representative images acquired by transmission electron microscopy at 10 days p.i. of 95
642 days old hCOs infected with a clade IIb lineage MPXV isolate with an MOI of 0.1 $TCID_{50}$/cell.
643 (b') Magnification demonstrating the presence of intracellular mature virions within cells. Scale
644 bar, 1 µm (b'') Magnification showing the presence of viral particles at different stages of
645 development alongside with perinuclear viral factories, displaying cytoskeletal condensations.
646 Scale bar, 1 µm. (c) Illustration of degenerative signs, bursting and release of intracellular
647 compartment containing high amounts of mpox virions. Scale bar, 1 µm. (d) MPXV particles
648 were observed localizing to neurites in infected hCO tissue. Black arrowheads indicate
649 exemplary virion-harboring neurites. Scale bar, 0.5 µm. (e) Representative image of the
650 detection by immunofluorescence of MPXV signal within neural filaments of interconnected,
651 distinct cells. MPXV, green; DAPI, blue. Scale bar, 10 µm. (f) Cell-associated and released
652 infectious MPXV 2 to 14 days p.i. of 70-95 days old hCOs infected with a clade IIb lineage
653 isolate at a rate of 0.1 $TCID_{50}$/cell. Boxplots indicate median value (centerline) and interquartile
654 ranges (box edges), with whiskers extending to the lowest and the highest values. Each symbol
655 represents an individual organoid (n=4-5 independent organoid batches). Mann-Whitney U test
656 was applied to compare groups. *$p<0.05$, **$p<0.01$. (g) Data presented in (f) represented as
657 percentage of total infectious virus content.
658

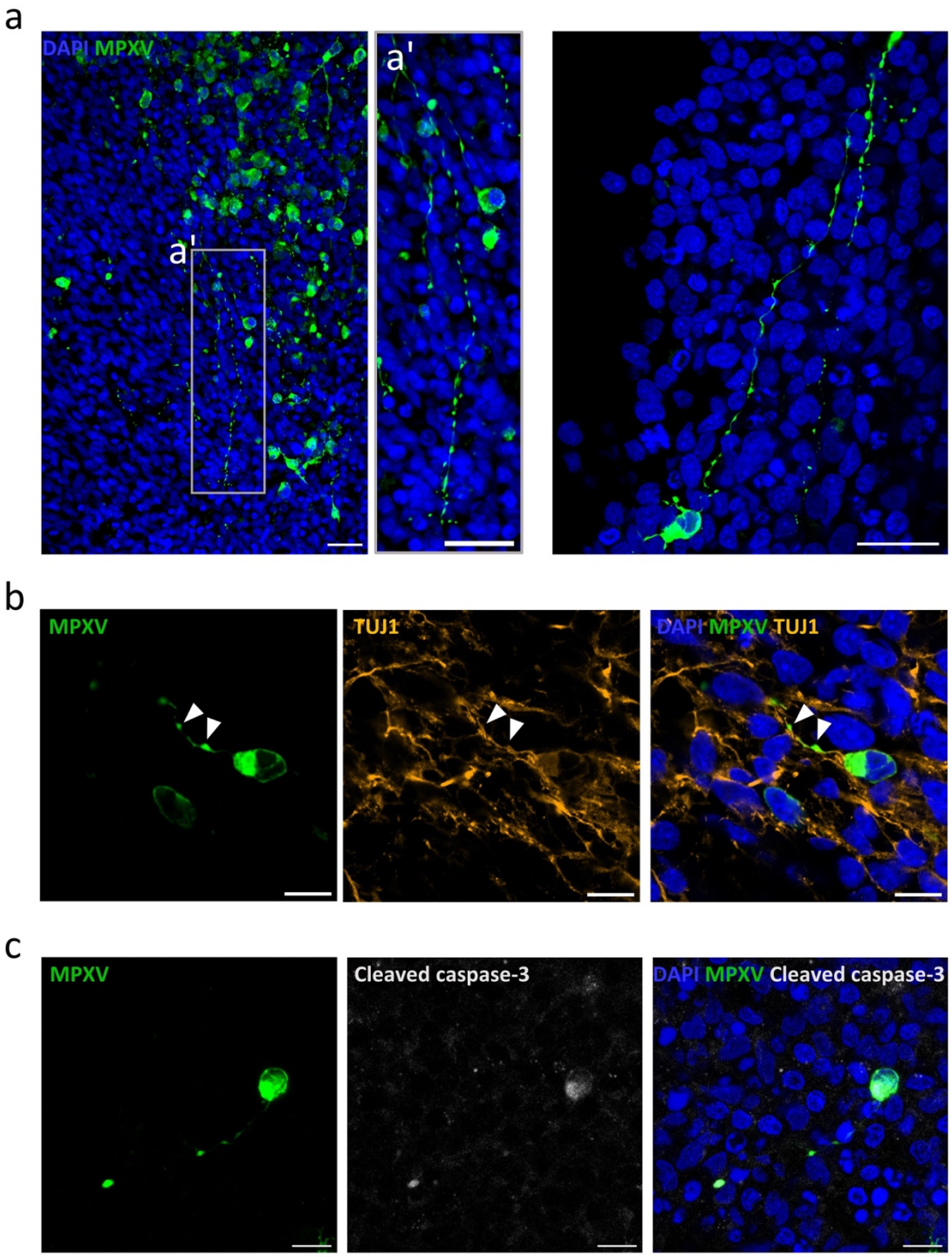

Figure 3: MPXV causes neuritic beading and injury in hCOs. (a-c) Immunofluorescene analysis 8-14 days p.i. of 70 days old hCOs exposed to a clade IIb lineage MPXV isolate at a rate of 0.1 $TCID_{50}$/cell. (a) Representative micrographs showing viral antigen accumulating within regularly interspaced swellings (beads) on filaments, spanning over long distances within the tissue. MPXV, green; DAPI, blue. Scale bar, 25 µm. (b) Representative micrographs of beaded filaments harboring mpox virions co-localizing with the neuronal marker TUJ1 in

666 both filaments and varicosities. MPXV, green; TUJ1, orange; DAPI, blue. Scale bar, 10 μm. (c)
667 Representative micrographs of neuritic beads and soma of an infected cell accumulating
668 cleaved caspase-3. MPXV, green; cleaved caspase-3, white; DAPI, blue. Scale bar, 10 μm.
669
670

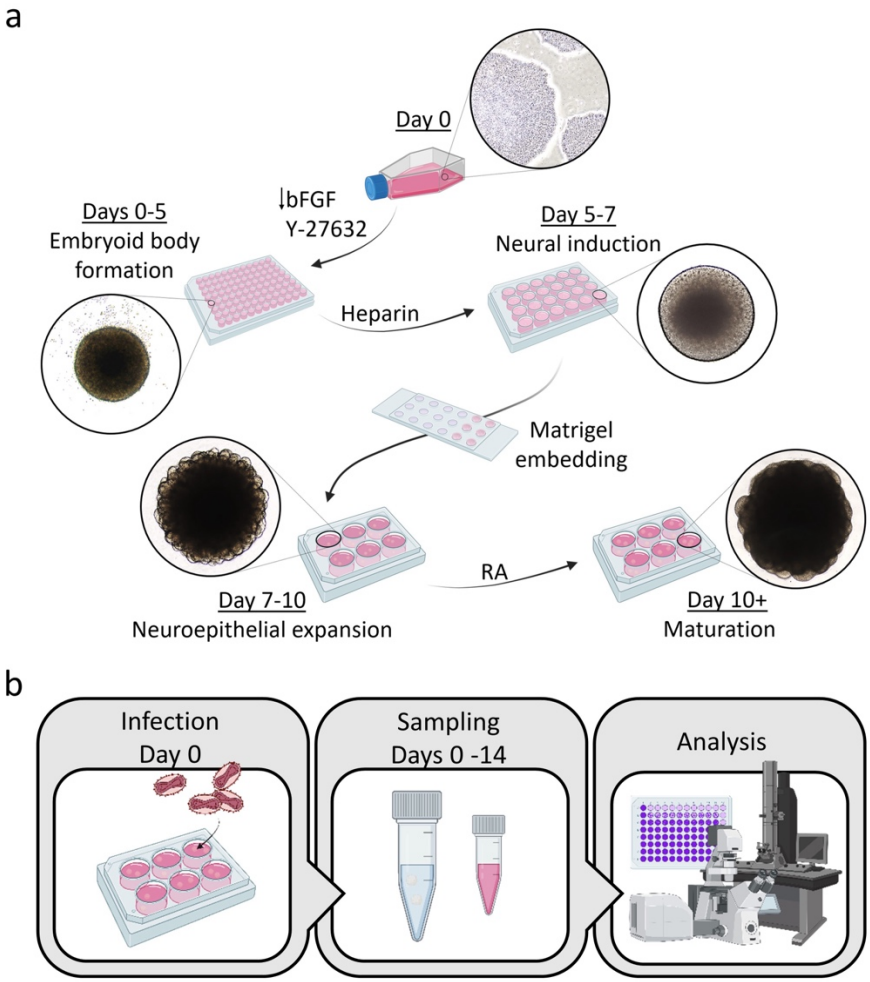

Supplementary Figure 1: Experimental design for hCOs generation and infection. (a) At day 0 ESCs were dissociated, resuspended in Formation Medium and distributed at a density of 9'000-10'000 cells per well in ultra-low attachment 96-well plates for EB formation. After 5 days, EBs were transferred to Induction Medium for neural induction. At day 7, EBs were embedded into Matrigel and transferred to ultra-low attachment 6-well plates in Expansion Medium. At day 10, hCOs were transferred to Maturation Medium and moved to an orbital shaker for further development. (b) 70 to 95 days old hCOs were infected with a clade IIb isolate at an MOI of 0.1 $TCID_{50}$/cell. Supernatant and tissue samples were taken at regular intervals for a period of up to 14 days, prior to analysis.

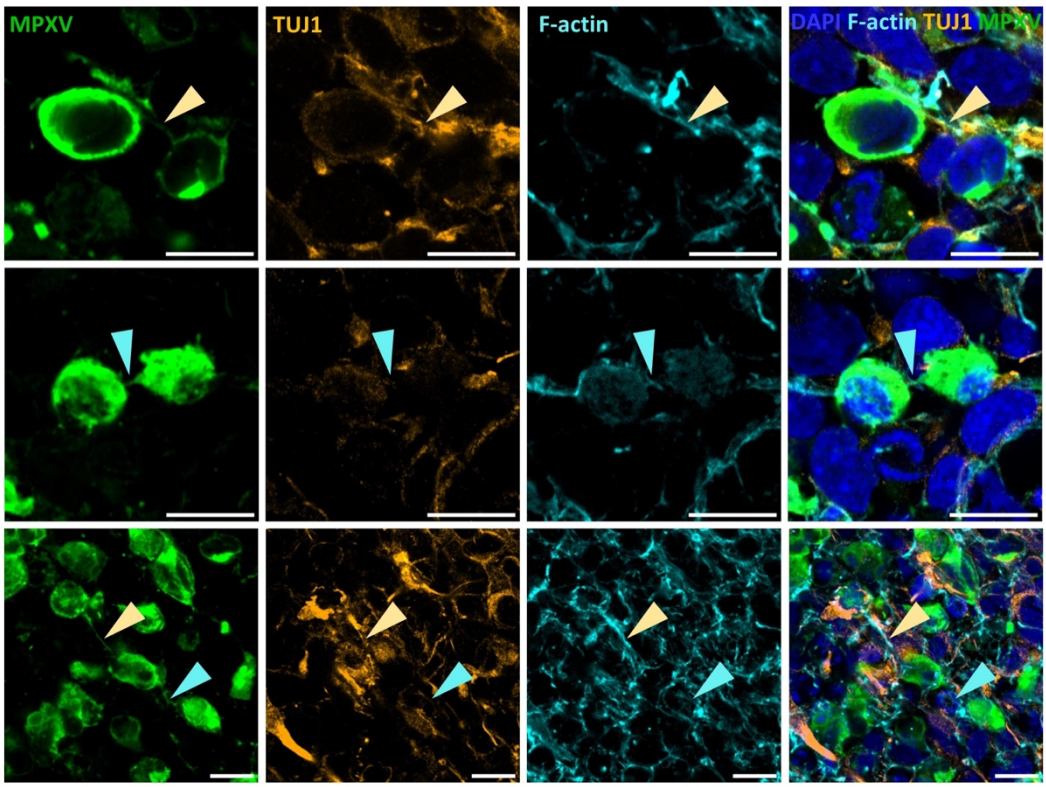

Supplementary Figure 2: Filaments interconnecting cells in hCOs comprise both TNTs and neurites. Representative micrographs showing the filaments connecting MPXV antigen positive cells and displaying diverse TUJ1 and F-actin patterns. Some filaments were observed showing expression of both markers (yellow arrowheads), indicative of their neuritic nature, others lacked TUJ1 signal, indicative of TNTs (blue arrowheads). MPXV, green; TUJ1, orange; F-actin, cyan blue; DAPI, dark blue. Scale bar, 10 μm.